

# Precessional pacing of tropical ocean carbon export during the Late Cretaceous

Ji-Eun Kim<sup>1</sup>, Thomas Westerhold<sup>2</sup>, Laia Alegret<sup>3</sup>, Anna Joy Drury<sup>4</sup>, Ursula Röhl<sup>2</sup>, Elizabeth M. Griffith<sup>1</sup>

<sup>1</sup>School of Earth Sciences, The Ohio State University, 43210 USA

5 <sup>2</sup>Center for Marine Environmental Sciences (MARUM), University of Bremen, 28359 Germany

<sup>3</sup>Department of Earth Sciences, University of Zaragoza, 50009 Spain

<sup>4</sup>Department of Earth Sciences, University College London, WC1E 6BT UK

*Correspondence to:* Elizabeth M. Griffith ([griffith.906@osu.edu](mailto:griffith.906@osu.edu)) and Thomas Westerhold ([twesterhold@marum.de](mailto:twesterhold@marum.de))

**Abstract.** The marine biological carbon pump, which exports organic carbon out of the surface ocean, plays an essential role in sequestering carbon from the atmosphere, thus impacting climate and affecting marine ecosystems. Orbital variations in solar insolation modulate these processes, but their influence on the tropical Pacific during the Late Cretaceous is unknown. Here we present a high-resolution composite record of elemental barium from deep sea sediments as a proxy for organic carbon export out of the surface oceans (i.e., export production) from Shatsky Rise in the tropical Pacific. Variations in export production in the Pacific during the Maastrichtian, from 71.5 to 66 million years ago, were dominated by precession and less so by eccentricity modulation or obliquity, confirming that tropical surface-ocean carbon dynamics were influenced by seasonal insolation in the tropics during this greenhouse period. We suggest that precession paced primary production in the tropical Pacific and recycling in the euphotic zone by changing water column stratification, upwelling intensity, and continental nutrient fluxes. Benthic foraminiferal accumulation rates covaried with export production providing evidence for benthopelagic coupling of the marine biological carbon pump across these high-frequency changes in a cool greenhouse planet.

## 20 **Short Summary**

This study attempts to get a better understanding of the marine biological carbon pump and ecosystem functioning under warmer than today conditions. Our records from marine sediments show the Pacific tropical marine biological carbon pump was driven by variations in seasonal insolation in the tropics during the Late Cretaceous and may play a key role in modulating climate and the carbon cycle globally in the future.

## 25 **1 Introduction**

High-resolution marine sedimentary records are important for shedding new light on critical aspects of Earth's climate and feedbacks in the ocean-atmosphere-biosphere system. On time scales of 10 thousand to 1 million years, variations in Earth's climate are paced by orbital (Milankovitch) cycles of eccentricity, obliquity and precession (e.g., 405 kyr, 100 kyr, 41 kyr, and

23-18 kyr) because they alter solar insolation and its distribution on Earth (Laskar et al., 2004, 2011). Orbital-scale climate  
30 change is well studied for the Cenozoic Era (e.g., Zachos et al., 2001; Westerhold et al., 2020), but there is limited  
understanding for earlier times prior to 66 million years. After peak hot greenhouse conditions of the Cretaceous during the  
Cenomanian about 100 million years ago (e.g., Forster et al., 2007; Huber et al., 2018), progressive global cooling ensued and  
continued until the end of the Cretaceous (Jenkyns et al., 1994; Friedrich et al., 2012; Voigt et al., 2012). Cool and warm  
periods were overlaid on the long-term climatic cooling, e.g., the early Maastrichtian cooling pulse (Haynes et al., 2020) and  
35 the warm mid-Maastrichtian event (Frank et al., 2005). Extinction of the globally distributed inoceramid bivalves also occurred  
following a peak in their abundance (e.g., MacLeod and Huber, 1996; Dameron et al., 2017). However, our understanding of  
the relationship between environmental and biotic change during this time is limited, in part due to the lack of records of key  
drivers of variability in the ocean-carbon-climate system at orbital timescales in key regions like the tropical Pacific.

Many lines of evidence including climate modeling studies suggest that low- and mid-latitude processes in the climate  
40 system respond in nonlinear ways to insolation forcing (e.g., Short et al., 1991; Crowley et al., 1992; Laepple and Lohmann,  
2009; Zeebe et al., 2017). In the low-latitudes, eccentricity-modulated precession is expected to dominate carbon cycle  
dynamics (Herbert et al., 1999; MacLeod et al., 2001). A key feedback driving these dynamics seems to relate to the global  
redistribution of moisture and energy by the hydrological cycle (e.g., Trenberth et al., 2000). Proxy records that provide  
evidence of carbon cycle dynamics, such as marine carbon isotope records ( $\delta^{13}\text{C}$ ), show dominant variability in the eccentricity  
45 (rather than precession) band. This effect could be due to the long residence time of carbon in Earth's exogenic system, which  
filters out higher resolution fluctuations (e.g., Pälike et al., 2006) or is related to orbitally paced phytoplankton evolution  
(Beaufort et al., 2022). Nonetheless, during the Late Cretaceous several records outside the tropical Pacific show precession-  
scale changes in sedimentology and bulk carbonate and foraminiferal carbon isotopes (Herbert et al., 1999; MacLeod et al.,  
2001; Batenburg et al., 2012, 2014; Barnet et al., 2018, 2019). Whether or not the tropical Pacific carbon cycle, which plays  
50 an important role in climate regulation as the largest ocean basin with high burial of pelagic biogenic sediment due to equatorial  
upwelling, was paced by precession is not clear. The resolution of existing records is insufficient to resolve precessional cycles  
(Jung et al., 2012, 2013; Voigt et al., 2012; Dameron et al., 2017). Without sufficient sampling resolution of existing records,  
high-frequency variability in the Earth system could potentially bias conclusions based on unrepresentative or less resolved  
records (e.g., Herbert et al., 1999).

55 Here we present an astronomically-tuned, high-resolution record of open ocean organic carbon export, the organic carbon  
flux out of the surface of the ocean or export production, in the tropical Pacific during the Maastrichtian from 71.5 to 66 million  
years ago (Fig. 1). Export production is a key organic carbon flux within the marine biological carbon pump which sequesters  
carbon from atmosphere to the deep ocean through biologically mediated processes. We use a new composite X-ray  
fluorescence (XRF) scanning barium (Ba) record as a proxy for export production by comparing it to pelagic marine barite  
60 extracted from discrete samples and excess- or bio-Ba measurements on the same samples from the same cores. Accumulation  
of pelagic marine barite and excess-Ba in deep-sea sediments have been shown to correlate with organic carbon flux out of the  
photic zone (Paytan et al., 1996; Eagle et al., 2003), making these good proxies for export production where there is low

terrigenous input and sediment is not sulfate-reducing. We also reconstruct benthic foraminiferal assemblages and accumulation rates over two windows of time to test the relationship between organic carbon export from the surface ocean represented by the Ba records and organic carbon reaching the seafloor (i.e., the sequestration flux) represented by the benthic foraminiferal records. These new records allow us to better characterize the marine biological pump at this time and show that precession, rather than eccentricity or obliquity, was the dominant orbital cycle that paced ocean export production thereby influencing the marine carbon cycle in the tropics during the Maastrichtian cool greenhouse period.

## 2 Materials and methods

### 70 2.1 Study Site

Shatsky Rise formed about 145 million years ago in the Pacific (Larson et al., 1992; Sager et al., 1999), providing an archive of Cretaceous sediments in the tropics thought to have been above the carbonate compensation depth (CCD) between 1500 to 2000 m throughout their deposition (Sager et al., 1999). The current location of Ocean Drilling Program (ODP) Leg 198 Sites 1209 and 1210 are 32°39.1081'N, 158°30.3564'E (2387 m below sea level) and 32°13.420'N, 158°15.5623'E (2573 m below sea level), respectively (Bralower et al., 2002). Shatsky Rise drifted northward on the Pacific plate to its present location (Larson et al., 1992; Dameron et al., 2017). During the Late Cretaceous, Shatsky Rise was approximately 10°N of the equator (Fig. 1; Larson et al., 1992; Dameron et al., 2017) in a region of relatively high productivity due to upwelling caused by the divergence of the North Equatorial Counter Current and the North Equatorial Current. Previous studies on the Maastrichtian at Sites 1209 and 1210 identified the inoceramid acme and extinction, changes in ocean circulation, carbonate dissolution and episodes of higher productivity prior to the end-Cretaceous extinction event 66.0 million years ago (Bralower et al., 2002; Frank et al., 2005; Alegret and Thomas, 2009; Jung et al., 2012, 2013; Renne et al., 2013; Dameron et al., 2017). However, prior age models (Fig. S1) and data resolution were incomplete and insufficient to identify precessional cycles in these open ocean tropical Pacific sedimentary records.

### 2.2 Samples

85 This study used deep-sea marine sediment samples from ODP Leg 198 Sites 1209 and 1210 on Shatsky Rise, Northwest Pacific during the Maastrichtian (from 71.5 to 66 million years ago) to create a continuous composite record. Samples consisted primarily of very pale orange to white nannofossil ooze, mostly > 96 weight percent (wt %) CaCO<sub>3</sub>, and discontinuous chert nodules likely formed by remobilized biogenic silica (Bralower et al., 2002). Bulk carbonate  $\delta^{18}\text{O}$  and  $\delta^{13}\text{C}$  were measured in 1394 samples from both Sites 1209 (1096) and 1210 (298) about every 5 cm. Discrete samples from 5 intervals that consist of 90 51 samples in total included Samples 1209C-16H-1, 114 to 145 cm, -21H-1, 67 to 118 cm, -22H-2, 133 to -3, 31 cm, Sample 1209B-29H-1, 87 cm to -2, 20 cm, and Sample 1210B-25H-4, 43 to 80 cm. Samples were taken every 5 cm or so in the core and weigh between 13 to 22 g (approximately 20 cm<sup>3</sup>). Additional samples for benthic foraminifera were taken from over 2 of the 5 intervals that have barite data.

### 2.3 Bulk stable carbon and oxygen isotopes

95 Bulk carbonate  $\delta^{13}\text{C}$  and  $\delta^{18}\text{O}$  analyses (Datasets S1-S3) on 1394 freeze-dried and pulverized sediment samples from Sites  
1209 (1096) and 1210 (298) were performed at MARUM, University Bremen. The bulk stable carbon and oxygen isotope data  
are reported relative to the Vienna Pee Dee Belemnite (VPDB) international standard, determined via adjustment to calibrated  
in-house standards and NBS-19. Bulk carbonate analyses were carried out on a Finnigan MAT 251 mass spectrometer equipped  
with automated carbonate preparation line (Kiel III). Carbonate was reacted with orthophosphoric acid at 75 °C. Analytical  
100 precision based on replicate analyses of in-house standard (Solnhofen Limestone) is 0.04‰ (1 $\sigma$ ) for  $\delta^{13}\text{C}$  and 0.07‰ (1 $\sigma$ ) for  
 $\delta^{18}\text{O}$ .

### 2.4 Scanning XRF Ba

Non-destructive X-ray fluorescence (XRF) data were collected every 2 cm down-core using XRF core scanner Avaatech serial  
no. 17 from the XRF core scanning facility at the IODP Gulf Coast Repository at Texas A&M University (College Station,  
105 USA) in March 2017 for Sites 1209 and 1210 (Datasets S4-S6). Data were collected over a 1.2 cm<sup>2</sup> area with a down-core slit  
size of 10 mm using generator settings of 50 kV and a current of 0.75 mA, ideally for detecting Ba, and a sampling time of 12  
s in each run directly at the split core surface of the archive half. The split core surface was covered with a 4  $\mu\text{m}$  thin SPEXCerti  
Prep Ultralene foil to avoid contamination of the XRF detector prism and desiccation of the cores. The data were acquired  
with a SiriusSD 65mm<sup>2</sup> Silicon Drift Detector Model 878-0616B - SGX Sensortech with 133 eV X-ray resolution at 5.9keV  
110 and 3keps, the Canberra digital spectrum analyzer DAS 1000, and an Oxford Instruments 50W Neptune X-ray tube with a  
rhodium (Rh) target. Raw data spectra were processed using the Analysis of X-ray spectra by Iterative Least square software  
(bAxil) package from Canberra Eurisys. The scanning XRF Ba was used as a qualitative record of changes in biogenic barium  
flux at this open ocean setting after assessing minimal difference between XRF Ba and XRF Ba normalized to 'total area' (the  
sum of all counts for all elements processed from the 50 kV run data) (XRF Ba/total area) as shown in Fig. S2 to confirm that  
115 there is little to no volume effect on scanning XRF Ba trends. Additionally, XRF Sr/total area ratio (Fig. S3) is shown.

### 2.5 Composite Record

The scanning XRF Ba elemental intensities were used to correlate Maastrichtian cores from ODP Leg 198 Holes 1209A,  
1209B and 1209C as well as Holes 1210A and 1210B to establish new composite records for Site 1209 and 1210 (Figs. S4-  
S6). Additionally, all core intervals outside the composite were mapped to the composite to place data from those intervals on  
120 the new splice. All relevant tables for composite constructions are given in Datasets S7-S9 for Site 1209 and Datasets S10-  
S12 for Site 1210. To form a complete Maastrichtian succession both sites had to be combined to cover gaps and avoid drilling  
disturbed intervals. Correlation tie points using XRF Ba elemental intensities (Fig. S6) are given in Dataset S13.

## 2.6 Barite accumulation rate (BAR)

Barite separation was done on all 51 discrete sediment samples across 5 intervals (Dataset S14). The barite separation method, which dissolves carbonates, organic matter, Fe-Mn oxyhydroxides, silicates, and fluorides to obtain a purified barite residue, was modified from Paytan et al. (1996) as outlined in the Supplement Table S1. Specifically, acetic acid was used to slowly (but completely) dissolve carbonates because the samples had such high carbonate content (> 96 wt %). Sample ashing in a furnace to remove refractory organic material was done after the scanning electron microscope (SEM) observation due to the low weight of the residue (and low organic material content). Previous work (Eagle et al., 2003) showed that the barite separation method of Paytan et al. (1996) resulted in less than 5% loss of original barite when followed accordingly. Each sample residue was then imaged using a Hitachi Benchtop SEM TM3030 at Kent State University to determine the average percentage of barite (i.e., purity) by taking images of five random spots (Fig. S7). The purity was multiplied by the dry weight of the residue and divided by the total dry bulk sample weight to determine the pelagic marine barite wt %.

Barite accumulation rate (BAR) was then calculated by multiplying the pelagic marine barite wt % by the mass accumulation rate (MAR). This corrects any bias using wt % data that could result from varying linear sedimentation rate (LSR) or changes in dry bulk density (DBD). To determine the MAR, linear sedimentation rate (LSR) was multiplied by dry bulk density (DBD) from Bralower et al. (2002). Dry density in each core section was used where available, such as for Core section 198-1210B-25H-4. When there was no dry density measured for the specific core section, nearby dry density average was taken (1209B-27H-6 and -31H-1 DBD were used for 1209B-29H-1 and -2 and 1209C-21H-1) or nearest DBD was adopted (1209A-26H-4 was used for 1209C-16H; 1209B-31H-6 DBD was used for 1209C-22H- 2 and -3).

## 2.7 Excess-Ba (bio-Ba) accumulation rate (excess-BaAR)

Bulk digestion of aliquots of the same discrete bulk samples used for barite separation above was done to determine excess-Ba (i.e., biogenic Ba) content from measurements of Ba and Al (Dataset S15). A modified bulk digestion method from Scudder et al. (2014) was used as outlined in the Supplement Table S2 and the resulting solution was measured using a Perkin Elmer 3000DV ICP-OES in the Trace Element Research Lab at The Ohio State University. Supplement Table S3 shows the wavelength for each element analyzed and relative standard deviation (2RSD), determined from replicate analyses of the medium standard solution (n = 7). Measurements were 4% (2RSD) for Ba. Other elements (Ca, Fe, Al, Ti, Mn, Mg, Sr, and K) had 2RSD ranging from 2 to 3%, but Si had 2RSD of 16%.

Excess-Ba was calculated using an equation (Supplement Text S1) from Dymond et al. (1992) which corrects for any contribution of non-biogenic Ba. For this study, terrigenous Ba/Al ratio ( $Ba/Al_{\text{terrigenous}}$ ) of 0.0037 was used (Reitz et al., 2004). Additional corrections for Ba associated with authigenic components and Fe-smectite using measurements of Mn and Fe (Olivarez Lyle and Lyle, 2006) were not needed as these corrections resulted in differences of 6% or less (on average 2% difference, see Supplement Text S1). Excess-Ba accumulation rate (excess-BaAR) was then calculated by multiplying the excess-Ba (in ppm) by the MAR as determined above.

## 155 2.8 Benthic foraminiferal data

For quantitative studies of benthic foraminifera (Dataset S16) 16 selected samples were taken from the cores of Site 1209 spanning several cycles observed in scanning XRF Ba data. Samples of 10 to 15 cm<sup>3</sup> were taken at the Gulf Core Repository (GRC), then oven dried <50°C overnight and washed using tap water over a 63µm sieve to extract the sand sized fraction at MARUM Bremen. Wet sieved samples were oven dried <50°C overnight and weighed to determine coarse fraction weight %.

160 Benthic foraminiferal quantitative analysis was carried out at University of Zaragoza based on representative splits of approximately 300 specimens larger than 63 µm. The percentages of individual taxa, species with agglutinated tests, and the Superfamily Buliminacea were calculated (Dataset S16). The Benthic Foraminiferal Accumulation Rates (BFARs) were calculated as a qualitative proxy for delivery of organic matter to the seafloor (Jorissen et al., 2007), using the number of benthic foraminifera per gram of sediment > 63 µm, the weight % of the sample > 63 µm, the linear sedimentation rate and  
165 the sediment density. BFARs are expressed as the number of benthic foraminifera (nr) accumulated per cm<sup>2</sup> and per kyr.

## 3 Astrochronology and Cyclostratigraphy

Using the shipboard biostratigraphic datums (Fig. S1) and time series analysis we find that the Shatsky Rise ODP Sites 1209 and 1210 composite bulk δ<sup>13</sup>C record reveals a strong imprint of the 405-kyr long eccentricity cycle (Fig. 2). For an initial 405 kyr age model the composite bulk δ<sup>13</sup>C record was filtered for the 405 kyr cycle in the depth domain (5 m bandpass filter using  
170 0.2 ± 0.06). Then the thirteen identified 405 kyr cycles were correlated to the Laskar et al. (2004) and Laskar (2020) cosine function with correlating maxima in the δ<sup>13</sup>C filter to minima in the cosine function (Fig. 3). This phase relationship follows the findings in the Zumaia section from the Basque Country in Northern Spain (Batenburg et al., 2012) and provides a basic 405-kyr stratigraphy without introducing short eccentricity, obliquity or precession component features into the records. The age tie points for the 405-kyr age model are in the Supplement Table S4. To test the completeness of the Shatsky Rise record,  
175 we used the tie points of Batenburg et al. (2012) updated for the Laskar cosine function for the Zumaia succession and plotted bulk δ<sup>13</sup>C records (Fig. S8, Supplement Table S5). The match of both records is remarkable, suggesting that both Zumaia and Shatsky Rise recorded global carbon cycle variations.

The power ratio method used here can be subjective and thus we tested the record with the more complex statistical tool of Correlation Coefficient (COCO) and Evolutionary Correlation Coefficient (eCOCO) embedded in the *Acycle* software  
180 package (Li et al., 2019). Using *Acycle* the results are indeed basically the same as those done by the more simplistic power ratio method showing a most likely sedimentation rate at ~1.3 cm/kyr (Fig. S9). The eCOCO method reveals a minor discrepancy at ~285 m, which corresponds to the depth between 405-kyr cycles labelled Maa5 and Maa6 in Fig. 3 (and Fig. S8). If we assume that there is one more 405-kyr cycle in this interval, the carbon isotope minimum at 68.3 Ma would not match the Zumaia record anymore. It should be pointed out here that the drill cores used are affected by coring disturbance to  
185 some extent, particularly when chert layers were encountered. For the composite record from Shatsky Rise, we tried to avoid these intervals whenever possible. Some disturbance and therefore misinterpretation of changes in cycle thickness can occur

using an automated analysis routine that assumes constant sedimentation rates. We thus use the power-ratio astronomically-tuned age model presented here to reconstruct at high-resolution open ocean organic carbon export in the tropical Pacific during the Maastrichtian from 71.5 to 66 Ma.

## 190 **4 Proxy results and discussion**

### **4.1 Export production proxies**

Pelagic marine barite weight percent (wt %) and excess-Ba determined on the same samples between 71.5 to 66 Ma are positively correlated (Fig. 4), confirming that excess-Ba represents the biogenic or pelagic marine barite formed in the water column within microenvironments of decaying organic matter (Paytan et al., 1996). For the same or neighbouring samples  
195 (within 1 cm), X-ray fluorescence (XRF) Ba also has a strong positive correlation with both pelagic marine barite and excess-Ba. After calculating and comparing accumulation rates of barite (BAR) and excess-Ba (excess-BaAR) to scanning XRF Ba, the strong positive correlation remains (Fig. S10). This confirms that all barium records represent changes in export production in these sediments.

The equivalent barite accumulation from excess barite measurements, however, is higher than that determined from  
200 extracting barite. Either non-barite (i.e., non-biogenic) Ba phases are included in the excess-Ba data biasing the data (Murray et al., 2000; Eagle et al., 2003; Gonneea and Paytan, 2006) or BAR is underestimating barite accumulation due to the mechanical loss of barite or its dissolution during sample processing, which is possible for samples with low barite wt % (Eagle et al., 2003). Such offsets between proxies are a concern when trying to precisely quantify variations in proxy measurements in terms of export production. Nonetheless, offsets are less of a concern when looking at one site over time and comparing  
205 trends qualitatively to determine relative changes in export production, such as for this study. Therefore, we conclude that scanning XRF Ba is a valid proxy to reconstruct export production at high resolution in the open ocean tropical Pacific at Sites 1209 and 1210 during the Maastrichtian.

### **4.2 Orbital cyclicity in the tropical Pacific biological pump**

We observe orbital cyclicity in the continuous composite records of scanning XRF Ba and bulk carbonate  $\delta^{13}\text{C}$  and  $\delta^{18}\text{O}$   
210 from Sites 1209 and 1210 (Figs. 2, 5, and Figs. S11, S12). While the 405 kyr long-eccentricity used to constrain the age model dominates bulk carbonate  $\delta^{13}\text{C}$ , it is less dominant in bulk carbonate  $\delta^{18}\text{O}$  and least dominant in the scanning XRF Ba. This suggests that bulk carbonate  $\delta^{13}\text{C}$  is primarily responding to factors other than temperature or salinity and organic C export which impact the bulk carbonate  $\delta^{18}\text{O}$  and scanning XRF Ba, respectively. Because the bulk carbonate  $\delta^{13}\text{C}$  values closely resemble the lower resolution surface planktic foraminiferal  $\delta^{13}\text{C}$  record of *Rugoglobigerina rugosa* (Fig. S3) from the same  
215 sites reported by Jung et al. (2013), it is possible that it reflects surface conditions potentially related to local surface productivity. However additional high resolution work is needed to confirm this initial observation. The 100 kyr short-eccentricity cycle is weak in all three records and obliquity is not present in any of the records. Precession is observed in all

records but is strongest in XRF Ba, demonstrating that precession, not the modulating eccentricity cycle, played the major role in pacing organic C export or export production in the tropical Pacific during the Maastrichtian.

220 The variations in scanning XRF Ba throughout the composite record are interpreted as variations in export production and provide robust evidence for a tropical Pacific Ocean dominated by low-latitude (precessional) climate variations which responded strongly to precession even when the amplitude was low (e.g., during 100kyr eccentricity minima). When combined with existing records from the Atlantic during the Late Cretaceous (e.g., Herbert et al., 1990, 1999; MacLeod et al., 2001; Batenburg et al., 2012, 2014), a significant response of the Earth system due to the orbital forcing of precession is clear (Herbert  
225 et al., 1999; Clement et al., 2004).

The BAR and excess-BaAR records show export production increased by a factor of two to four within a single precessional cycle, in step with changes in scanning XRF Ba (Fig. 6, and Fig. S13). These large changes in the flux of organic matter falling through the water column can be caused by changes in surface production, transport efficiency, or both (Murray et al., 1996; Griffith et al., 2021). This data also suggests that these sites had generally low rates of new production (<2.2 gC  
230 cm<sup>2</sup> yr<sup>-1</sup> using Dymond et al. (1992), see Supplement Text S2) or that a very small fraction of the surface production was exported to depth (i.e., low transfer efficiency).

During these same precessional cycles, the barite related proxies are in phase with the amount of exported organic matter that reaches the seafloor (i.e., sequestration flux), reconstructed using benthic foraminifera accumulation rates (BFARs; e.g., Alegret et al., 2012, 2020; Griffith et al., 2021) (Fig. 6). A similar trend is shown in the percentage of the Superfamily  
235 Buliminacea, which in the absence of low-oxygen conditions is indicative of enhanced food supply to the seafloor (Jorissen et al., 2007; Alegret et al., 2012), and the percentage of the oligotrophic species *Oridorsalis umbonatus* is higher when Ba drops in the intervals of low export productivity (Fig. S14). These results suggest coupling between export production and carbon sequestration (i.e., carbon reaching the seafloor) in the tropical Pacific open ocean during the Maastrichtian. The variability in these short but high-resolution records is similar to that of lower resolution records (e.g., Frank et al., 2005), suggesting that  
240 caution is needed when interpreting lower resolution records of a highly variable signal, where drivers of variability can be masked in the lower resolution records.

#### 4.3 Direct response to precession during greenhouse

Carbon export from the surface ocean in the tropical Pacific (evidenced by XRF-Ba content) appears to have changed as a direct response to high frequency (~21 kyr) seasonal, insolation forced tropical precipitation. This fingerprint of precession in  
245 the deep-sea sedimentary record is most simply explained as the result of variations in surface productivity forced by cyclic variation in water column stratification, upwelling intensity, and continental nutrient fluxes. In the tropical Pacific, where the thermocline depth has a strong influence on ocean primary production (Turk et al., 2001), a ~21 kyr precession cycle could have been dominant in the Maastrichtian (Fig. 7). Shoaling of the thermocline would result in increased primary production and carbon export due to enhanced upwelling of nutrients, and this new record suggests such variations could have occurred  
250 in response to changes in precession. Previous work suggested a link between past warm climates and a “permanent El Niño”



state (Wara et al., 2005; Fedorov et al., 2006) with weak trade winds along the equator, a deeper thermocline and more stratified tropical Pacific preventing upwelling of nutrients, which resulted in reduced primary production and low carbon export. Today this scenario occurs as an irregular periodic variation along with an opposite “La Niña” state in the tropical Pacific with strong trade winds and more intense upwelling in the eastern tropical Pacific driving increased productivity on interannual-to-decadal timescales. Changes in the mean state over longer timescales can be recorded in deep sea sediment archives (e.g., Pena et al., 2008; Zhang et al., 2021). The large range of variations in our carbon export record in the tropical Pacific (XRF-Ba elemental intensities and benthic foraminiferal accumulation rates) during the Maastrichtian greenhouse argues against the hypothesis of a continual or permanent El Niño-like state. Our record exhibits variations which could reflect changes in the mean climate state. We suggest that this new record adds to the growing body of evidence that suggests robust El Niño-Southern Oscillation-like variability existed in past greenhouse conditions (e.g., Davies et al., 2012) and this ENSO-like variability may be sensitive to orbital forcing, especially the effect of orbital precession in the tropics (e.g., Clement et al., 1999; 2000; Lu et al., 2019). The resulting tropical mean climate state and climate variability forced by precession minima or maxima changing the strength of coupled ocean-atmosphere feedbacks in the tropical Pacific is less clear during the Maastrichtian greenhouse (Fig. 7), and requires focused modelling efforts and new proxy records to test these hypothesized relationships.

Reduced stratification and enhanced upwelling increase primary production and organic carbon export, but are expected to induce a greater release of CO<sub>2</sub> to the atmosphere and act as a positive feedback to warming, unless the enhanced biological pump effectively suppresses the increase in CO<sub>2</sub> outgassing due to enhanced upwelling (e.g., Kim et al., 2019). Increased organic carbon export would also increase the corrosivity of deeper waters (e.g., Lyle et al., 1995), although CaCO<sub>3</sub> content in sediments remained high throughout this time at this site (>95%; Dataset S14). The maxima in corrosion-resistant benthic foraminifera (*N. truempyi*) and percent of agglutinated taxa, however, coincide with Ba maxima providing further support of increased organic carbon export (Fig. S14).

The high frequency, precessional pacing of the carbon export in the tropical Pacific persisted throughout the Maastrichtian. This suggests it was a consistent, intrinsic feature of the end Cretaceous cool greenhouse, despite longer (and larger) scale changes, e.g., early Maastrichtian cooling pulse (EMCP; Haynes et al., 2020), warm mid-Maastrichtian event (MME; MacLeod and Huber, 1996), the early phase of Deccan Traps Volcanism (67.5 to 67.1 Ma; Chenet et al., 2007; Keller et al., 2016), or the Latest Maastrichtian Warming Event (LMWE; Li & Keller, 1998; Gilabert et al., 2021). Organic carbon export appears largely decoupled from the abundance and eventual extinction of inoceramid bivalves related to the MME, suggesting that additional drivers (e.g., emplacement of large igneous provinces) played an important role in biotic change during this time. An increase in amplitude of the variations in carbon export recorded towards the end of the Cretaceous suggests an amplified sensitivity to orbital forcing when CO<sub>2</sub> was higher during Deccan volcanism, beginning around 67.5 Ma (Chenet et al., 2007).

As anthropogenic CO<sub>2</sub> emissions increase today, we need to consider whether or not sensitivity to seasonal insolation in the tropics might increase and dominate changes in the ocean-carbon-climate system in this key region.

**Data availability.** All data are available in the Supplement and will be available at [www.pangaea.de](http://www.pangaea.de) upon approval.

285

**Supplement.** The supplement related to this article will be available online at: *insert link to Climate of the Past Supplement file.*

**Author contributions.** All authors contributed to the ideas expressed in this manuscript. TW initiated this project, which was further developed by EMG, and J-EK; TW and UR analyzed XRF and bulk carbonate isotopes; J-EK prepared and analyzed barite samples under the guidance of EMG; LA prepared and analyzed the benthic foraminiferal results. TW created the age model and composite record. J-EK, EMG, TW, LA and AJ did the artwork. All authors contributed to data interpretation and manuscript writing.

295 **Competing interests.** The contact author has declared that neither they nor their co-authors have any competing interests.

**Disclaimer.** Publisher's note: Copernicus Publications remains neutral with regard to jurisdictional claims in published maps and institutional affiliations.

300 **Acknowledgements.** Samples were provided by the International Ocean Drilling Program. We thank the staff at the IODP Gulf Coast Core Repository (GCR) for assistance at the Texas A&M University XRF Core Scanner Lab and sampling guidance. We also thank Faizura Ahmad Zulkifli and Anis Hishammudin for assistance in barite separation, Samantha Carter for supervision on the separation process, Julia Sheets and Susan Welch for supervision on SEM sample coating, Anthony Lutton for supervision on ICP measurements, Merida Keatts at Kent State University for supervision on the SEM operation, and Jason Curtis at University of Florida for processing the carbonate weight percent.

310 **Financial support.** Funding for this research was provided by the Deutsche Forschungsgemeinschaft (DFG, German Research Foundation) to TW and UR - project no. 320221997, and by grant PID2019-105537RB-I00 funded by MCIN/AEI/10.13039/501100011033 and by "ERDF A way of making Europe" to LA. Funding was also provided by the Deutsche Forschungsgemeinschaft (DFG, German Research Foundation) under Germany's Excellence Strategy – EXC-2077 – 390741603. This work was also supported in part by Ohio State Friends of Orton Hall to J-EK and US National Science Foundation grant OCE-1536630 to EMG.

## References

- 315 Alegret, L. and Thomas, E.: Food supply to the seafloor in the Pacific Ocean after the Cretaceous/Paleogene boundary event, *Mar. Micropaleontol.*, 73, 105–116, <https://doi.org/10.1016/j.marmicro.2009.07.005>, 2009.
- Alegret, L., Thomas, E., and Lohmann, K. C.: End-Cretaceous marine mass extinction not caused by productivity collapse, *Proc. Natl. Acad. Sci.*, 109, 728–732, <https://doi.org/10.1073/pnas.1110601109>, 2012.
- Alegret, L., Arreguín-Rodríguez, G. J., Trasviña-Moreno, C. A., and Thomas, E.: Turnover and stability in the deep sea: Benthic foraminifera as tracers of Paleogene global change, *Glob. Planet. Change*, 103372, 2020.
- 320 Barnet, J. S., Littler, K., Kroon, D., Leng, M. J., Westerhold, T., Röhl, U., and Zachos, J. C.: A new high-resolution chronology for the Late Maastrichtian warming event: Establishing robust temporal links with the onset of Deccan volcanism, *Geology*, 46, 147–150, 2018.
- Barnet, J. S., Littler, K., Westerhold, T., Kroon, D., Leng, M. J., Bailey, I., Röhl, U., and Zachos, J. C.: A high-fidelity benthic stable isotope record of Late Cretaceous–Early Eocene climate change and carbon-cycling, *Paleoceanogr. Paleoclimatology*, 34, 672–691, 2019.
- 325 Batenburg, S. J., Sprovieri, M., Gale, A. S., Hilgen, F. J., Hüsing, S., Laskar, J., Liebrand, D., Lirer, F., Orue-Etxebarria, X., and Pelosi, N.: Cyclostratigraphy and astronomical tuning of the Late Maastrichtian at Zumaia (Basque country, Northern Spain), *Earth Planet. Sci. Lett.*, 359, 264–278, 2012.
- Batenburg, S. J., Gale, A. S., Sprovieri, M., Hilgen, F. J., Thibault, N., Boussaha, M., and Orue-Etxebarria, X.: An astronomical time scale for the Maastrichtian based on the Zumaia and Sopelana sections (Basque country, northern Spain), *J. Geol. Soc.*, 171, 165–180, 2014.
- 330 Beaufort, L., Bolton, C. T., Sarr, A.-C., Suchéras-Marx, B., Rosenthal, Y., Donnadieu, Y., Barbarin, N., Bova, S., Cornuault, P., Gally, Y., Gray, E., Mazur, J.-C., and Tetard, M.: Cyclic evolution of phytoplankton forced by changes in tropical seasonality, *Nature*, 601, 79–84, <https://doi.org/10.1038/s41586-021-04195-7>, 2022.
- 335 Bralower, T., Premoli Silva, I., and Malone, M.: Leg 198, Proceedings of the Ocean Drilling Program: Initial Reports, College Station, TX (Ocean Drilling Program), 2002.
- Chenet, A.-L., Quidelleur, X., Fluteau, F., Courtillot, V., and Bajpai, S.: 40K–40Ar dating of the Main Deccan large igneous province: Further evidence of KTB age and short duration, *Earth Planet. Sci. Lett.*, 263, 1–15, 2007.
- 340 Clement, A. C., Hall, A., and Broccoli, A. J.: The importance of precessional signals in the tropical climate, *Clim. Dyn.*, 22, 327–341, <https://doi.org/10.1007/s00382-003-0375-8>, 2004.
- Clement, A. C., Seager, R., and Cane, M. A.: Orbital controls on the El Niño/Southern Oscillation and the tropical climate, *Paleoceanography*, 14, 441–456, doi:10.1029/1999PA900013, 1999.
- Clement, A. C., Seager, R., and Cane, M. A.: Suppression of El Niño during the mid-Holocene by changes in the Earth's orbit, *Paleoceanography*, 15, 731–737, doi:10.1029/1999PA000466, 2000.

345

- Crowley, T. J., Kim, K.-Y., Mengel, J. G., and Short, D. A.: Modeling 100,000-Year Climate Fluctuations in Pre-Pleistocene Time Series, *Science*, 255, 705–707, 1992.
- 350 Dameron, S. N., Leckie, R. M., Clark, K., MacLeod, K. G., Thomas, D. J., and Lees, J. A.: Extinction, dissolution, and possible ocean acidification prior to the Cretaceous/Paleogene (K/Pg) boundary in the tropical Pacific, *Palaeogeogr. Palaeoclimatol. Palaeoecol.*, 485, 433–454, 2017.
- Davies, A., Kemp, A. E. S., Weedon, G. P., and Barron, J. A.: El Niño–Southern Oscillation variability from the Late Cretaceous Marca Shale of California, *Geology*, 40, 15–18, <https://doi.org/10.1130/G32329.1>, 2012.
- 355 Dymond, J., Suess, E., and Lyle, M.: Barium in deep-sea sediment: A geochemical proxy for paleoproductivity, *Paleoceanography*, 7, 163–181, 1992.
- Eagle, M., Paytan, A., Arrigo, K. R., van Dijken, G., and Murray, R. W.: A comparison between excess barium and barite as indicators of carbon export, *Paleoceanography*, 18, 2003.
- Fedorov, A. V., Dekens, P. S., McCarthy, M., Ravelo, A. C., deMenocal, P. B., Barreiro, M., Pacanowski, R. C., and Philander, S. G.: The Pliocene Paradox (Mechanisms for a Permanent El Niño), *Science*, 312, 1485–1489, <https://doi.org/10.1126/science.1122666>, 2006.
- 360 Forster, A., Schouten, S., Baas, M., and Sinninghe Damsté, J. S.: Mid-Cretaceous (Albian–Santonian) sea surface temperature record of the tropical Atlantic Ocean, *Geology*, 35, 919–922, 2007.
- Frank, T. D., Thomas, D. J., Leckie, R. M., Arthur, M. A., Bown, P. R., Jones, K., and Lees, J. A.: The Maastrichtian record from Shatsky Rise (northwest Pacific): A tropical perspective on global ecological and oceanographic changes, *Paleoceanography*, 20, 2005.
- 365 Friedrich, O., Norris, R. D., and Erbacher, J.: Evolution of middle to Late Cretaceous oceans—A 55 m.y. record of Earth’s temperature and carbon cycle, *Geology*, 40, 107–110, <https://doi.org/10.1130/g32701.1>, 2012.
- Gilabert, V., Arz, J. A., Arenillas, I., Robinson, S. A., and Ferrer, D.: Influence of the Latest Maastrichtian Warming Event on planktic foraminiferal assemblages and ocean carbonate saturation at Caravaca, Spain, *Cretac. Res.*, 125, 104844, <https://doi.org/10.1016/j.cretres.2021.104844>, 2021.
- 370 Gonneea, M. E. and Paytan, A.: Phase associations of barium in marine sediments, *Mar. Chem.*, 100, 124–135, 2006.
- Griffith, E. M., Thomas, E., Lewis, A. R., Penman, D. E., Westerhold, T., and Winguth, A. M.: Benthic–Pelagic Decoupling: The Marine Biological Carbon Pump During Eocene Hyperthermals, *Paleoceanogr. Paleoclimatology*, 36, e2020PA004053, 2021.
- 375 Grinsted, A., Moore, J. C., and Jevrejeva, S.: Application of the cross wavelet transform and wavelet coherence to geophysical time series, *Nonlinear Process. Geophys.*, 11, 561–566, 2004.
- Haynes, S. J., MacLeod, K. G., Ladant, J.-B., Guchte, A. V., Rostami, M. A., Poulsen, C. J., and Martin, E. E.: Constraining sources and relative flow rates of bottom waters in the Late Cretaceous Pacific Ocean, *Geology*, 48, 509–513, 2020.
- 380 Herbert, T. D. and D’Hondt, S. L.: Precessional climate cyclicity in Late Cretaceous—Early Tertiary marine sediments: a high resolution chronometer of Cretaceous–Tertiary boundary events, *Earth Planet. Sci. Lett.*, 99, 263–275, [https://doi.org/10.1016/0012-821X\(90\)90115-E](https://doi.org/10.1016/0012-821X(90)90115-E), 1990.

- Herbert, T. D., Gee, J., and DiDonna, S.: Precessional cycles in the Upper Cretaceous pelagic sediments of the South Atlantic: Long-term patterns from high-frequency climate variations, *Spec. Pap.-Geol. Soc. Am.*, 105–120, 1999.
- 385 Huber, B. T., MacLeod, K. G., Watkins, D. K., and Coffin, M. F.: The rise and fall of the Cretaceous Hot Greenhouse climate, *Glob. Planet. Change*, 167, 1–23, 2018.
- Jenkyns, H., Gale, A., and Corfield, R.: Carbon-and oxygen-isotope stratigraphy of the English Chalk and Italian Scaglia and its palaeoclimatic significance, *Geol. Mag.*, 131, 1994.
- Jorissen, F. J., Fontanier, C., and Thomas, E.: Chapter Seven Paleooceanographical Proxies Based on Deep-Sea Benthic Foraminiferal Assemblage Characteristics, in: *Developments in Marine Geology*, vol. 1, edited by: Hillaire-Marcel, C. and De Vernal, A., Elsevier, 263–325, [https://doi.org/10.1016/S1572-5480\(07\)01012-3](https://doi.org/10.1016/S1572-5480(07)01012-3), 2007.
- 390 Jung, C., Voigt, S., and Friedrich, O.: High-resolution carbon-isotope stratigraphy across the Campanian–Maastrichtian boundary at Shatsky Rise (tropical Pacific), *Cretac. Res.*, 37, 177–185, 2012.
- Jung, C., Voigt, S., Friedrich, O., Koch, M. C., and Frank, M.: Campanian-Maastrichtian ocean circulation in the tropical Pacific, *Paleoceanogr. Paleoclimatology*, 28, 562–573, 2013.
- 395 Keller, G., Punekar, J., and Mateo, P.: Upheavals during the Late Maastrichtian: Volcanism, climate and faunal events preceding the end-Cretaceous mass extinction, *Palaeogeogr. Palaeoclimatol. Palaeoecol.*, 441, 137–151, 2016.
- Kim, H. J., Kim, T., Hyeong, K., Yeh, S., Park, J., Yoo, C. M., and Hwang, J.: Suppressed CO<sub>2</sub> outgassing by an enhanced biological pump in the Eastern Tropical Pacific, *J. Geophys. Res. Oceans*, 124, 7962–7973, 2019.
- Laepple, T. and Lohmann, G.: Seasonal cycle as template for climate variability on astronomical timescales, *Paleoceanography*, 24, <https://doi.org/10.1029/2008PA001674>, 2009.
- 400 Larson, R., Steiner, M., Erba, E., and Lancelot, Y.: Paleolatitudes and tectonic reconstructions of the oldest portion of the Pacific plate: A comparative study, Larson, RL, Lancelot, Y., et al., *Proc. ODP, Sci. Results*, 615–631, 1992.
- Laskar, J.: Chapter 4 - Astrochronology, in: *Geologic Time Scale 2020*, edited by: Gradstein, F. M., Ogg, J. G., Schmitz, M. D., and Ogg, G. M., Elsevier, 139–158, <https://doi.org/10.1016/B978-0-12-824360-2.00004-8>, 2020.
- 405 Laskar, J., Robutel, P., Joutel, F., Gastineau, M., Correia, A., and Levrard, B.: A long-term numerical solution for the insolation quantities of the Earth, *Astron. Astrophys.*, 428, 261–285, 2004.
- Laskar, J., Fienga, A., Gastineau, M., and Manche, H.: La2010: a new orbital solution for the long-term motion of the Earth, *Astron. Astrophys.*, 532, A89, 2011.
- Li, M., Hinnov, L.A., and Kump, L.: *Acycle*: Time-series analysis software for paleoclimate research and education, *Computers and Geosciences*, 127, 12–21, 2019.
- 410 Li, L. and Keller, G.: Abrupt deep-sea warming at the end of the Cretaceous, *Geology*, 26, 995–998, 1998.
- Lu, Z., Liu, Z., Chen, G., and Guan, J.: Prominent precession band variance in ENSO intensity over the last 300,000 years, *Geophysical Research Letters*, 46, 9786–9795, [doi:10.1029/2019GL083410](https://doi.org/10.1029/2019GL083410), 2019.

- 415 Lyle, M., Dadey, K. A., and Farrell, J. W.: The Late Miocene (11–8 Ma) eastern Pacific carbonate crash: evidence for reorganization of deep-water circulation by the closure of the Panama Gateway, 1995 Proc. Ocean Drill. Program Sci. Results, 138, 821–837, 1995.
- MacLeod, K. G. and Huber, B. T.: Reorganization of deep ocean circulation accompanying a Late Cretaceous extinction event, *Nature*, 380, 422, 1996.
- 420 MacLeod, K. G., Huber, B. T., Pletsch, T., Röhl, U., and Kucera, M.: Maastrichtian foraminiferal and paleoceanographic changes on Milankovitch timescales, *Paleoceanography*, 16, 133–154, 2001.
- Murray, J. W., Young, J., Newton, J., Dunne, J., Chapin, T., Paul, B., and McCarthy, J. J.: Export flux of particulate organic carbon from the central equatorial Pacific determined using a combined drifting trap-<sup>234</sup>Th approach, *Deep Sea Res. Part II Top. Stud. Oceanogr.*, 43, 1095–1132, 1996.
- 425 Murray, R. W., Knowlton, C., Leinen, M., Mix, A. C., and Polsky, C.: Export production and carbonate dissolution in the central equatorial Pacific Ocean over the past 1 Myr, *Paleoceanography*, 15, 570–592, 2000.
- Olivarez Lyle, A. and Lyle, M. W.: Missing organic carbon in Eocene marine sediments: Is metabolism the biological feedback that maintains end-member climates?, *Paleoceanography*, 21, 2006.
- 430 Pälke, H., Norris, R. D., Herrle, J. O., Wilson, P. A., Coxall, H. K., Lear, C. H., Shackleton, N. J., Tripathi, A. K., and Wade, B. S.: The heartbeat of the Oligocene climate system, *Science*, 314, 1894–1898, <https://doi.org/10.1126/science.1133822>, 2006.
- Paytan, A., Kastner, M., and Chavez, F.: Glacial to interglacial fluctuations in productivity in the equatorial Pacific as indicated by marine barite, *Science*, 274, 1355–1357, 1996.
- Pena, L. D., Cacho, I., Ferretti, P., and Hall, M. A.: El Niño-Southern Oscillation-like variability during glacial terminations and interlatitudinal teleconnections, *Paleoceanography*, 23, PA3101, doi:10.1029/2008PA001620, 2008.
- 435 Reitz, A., Pfeifer, K., De Lange, G., and Klump, J.: Biogenic barium and the detrital Ba/Al ratio: a comparison of their direct and indirect determination, *Mar. Geol.*, 204, 289–300, 2004.
- Renne, P.R., Deino, A.L., Hilgen, F.J., Kuiper, K.F., Mark, D.F., Mitchell, W.S., Morgan, L.E., Mundil, R., and Smit, J.: Time scales of critical events around the Cretaceous-Paleogene boundary, *Science*, 339, 684–687, 2013.
- 440 Sager, W. W., Kim, J., Klaus, A., Nakanishi, M., and Khankishieva, L. M.: Bathymetry of Shatsky Rise, northwest Pacific Ocean: Implications for ocean plateau development at a triple junction, *J. Geophys. Res. Solid Earth*, 104, 7557–7576, 1999.
- Scotese, C. R. and Wright, N.: PALEOMAP Paleodigital Elevation Models (PaleoDEMS) for the Phanerozoic, [www.earthbyte.org/webdav/ftp/Data\\_Collections/Scotese\\_Wright\\_2018\\_PaleoDEM/Scotese\\_Wright2018\\_PALEOMAP\\_PaleoDEMs.pdf](http://www.earthbyte.org/webdav/ftp/Data_Collections/Scotese_Wright_2018_PaleoDEM/Scotese_Wright2018_PALEOMAP_PaleoDEMs.pdf), 2018.
- 445 Scudder, R. P., Murray, R. W., Schindlbeck, J. C., Kutterolf, S., Hauff, F., and McKinley, C. C.: Regional-scale input of dispersed and discrete volcanic ash to the Izu-Bonin and Mariana subduction zones, *Geochem. Geophys. Geosystems*, 15, 4369–4379, 2014.
- Short, D. A., Mengel, J. G., Crowley, T. J., Hyde, W. T., and North, G. R.: Filtering of Milankovitch cycles by Earth’s geography, *Quat. Res.*, 35, 157–173, 1991.

Torrence, C. and Compo, G. P.: A Practical Guide to Wavelet Analysis, *Bull. Am. Meteorol. Soc.*, 79, 61–78, 1998.

450 Trenberth, K. E., Stepaniak, D. P., and Caron, J. M.: The global monsoon as seen through the divergent atmospheric circulation, *J. Clim.*, 13, 3969–3993, 2000.

Turk, D., McPhaden, M. J., Busalacchi, A. J., and Lewis, M. R.: Remotely sensed biological production in the Equatorial Pacific, *Science*, 293, 471–474, <https://doi.org/10.1126/science.1056449>, 2001.

455 Voigt, S., Gale, A. S., Jung, C., and Jenkyns, H. C.: Global correlation of Upper Campanian–Maastrichtian successions using carbon-isotope stratigraphy: development of a new Maastrichtian timescale, *Newsl. Stratigr.*, 45, 25–53, 2012.

Wara, M. W., Ravelo, A. C., and Delaney, M. L.: Permanent El Nino-like conditions during the Pliocene warm period, *Science*, 309, 758–761, 2005.

460 Westerhold, T., Marwan, N., Drury, A. J., Liebrand, D., Agnini, C., Anagnostou, E., Barnet, J. S., Bohaty, S. M., De Vleeschouwer, D., and Florindo, F.: An astronomically dated record of Earth’s climate and its predictability over the last 66 million years, *Science*, 369, 1383–1387, 2020.

Zachos, J., Pagani, M., Sloan, L., Thomas, E., and Billups, K.: Trends, rhythms, and aberrations in global climate 65 Ma to present, *Science*, 292, 686–693, 2001.

Zeebe, R. E., Westerhold, T., Littler, K., and Zachos, J. C.: Orbital forcing of the Paleocene and Eocene carbon cycle, *Paleoceanography*, 32, 440–465, 2017.

465 Zhang, S., Yu, Z., Gong, X., Wang, Y., Chang, F., Lohmman, G., Qi, Y., and Li, T.: Precession cycles of the El Niño/Southern oscillation-like system controlled by Pacific upper-ocean stratification, *Communications Earth & Environment*, 2, 239, [doi:10.1038/s43247-021-00305-05](https://doi.org/10.1038/s43247-021-00305-05), 2021.

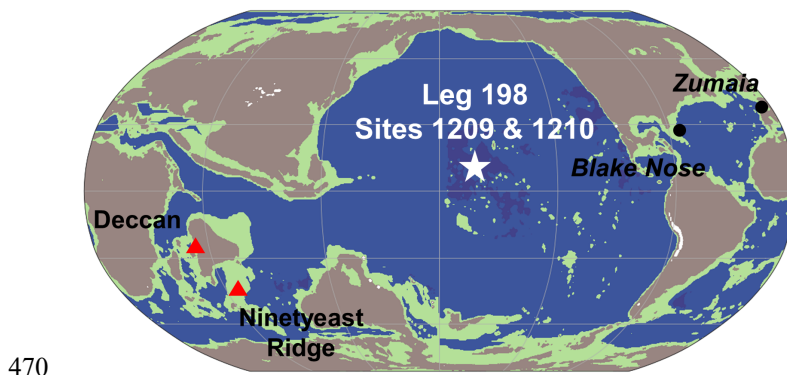


**Figure 1: Location of ODP Leg 198 Sites 1209 and 1210 at Shatsky Rise at 69 Ma (star) in the tropical Pacific (Scotese and Wright, 2018). Deccan and Ninetyeast Ridge are shown as red triangles. Location of Zumaia (Batenburg et al., 2012, 2014) and Blake Nose (MacLeod et al., 2001) records are shown as black circles. Shading indicates land above 0 m (brown), land above 6 km (white), and ocean settings with water depths greater than 4km (dark blue), between 4km and 120 m (blue), and above 120 m (green).**

475

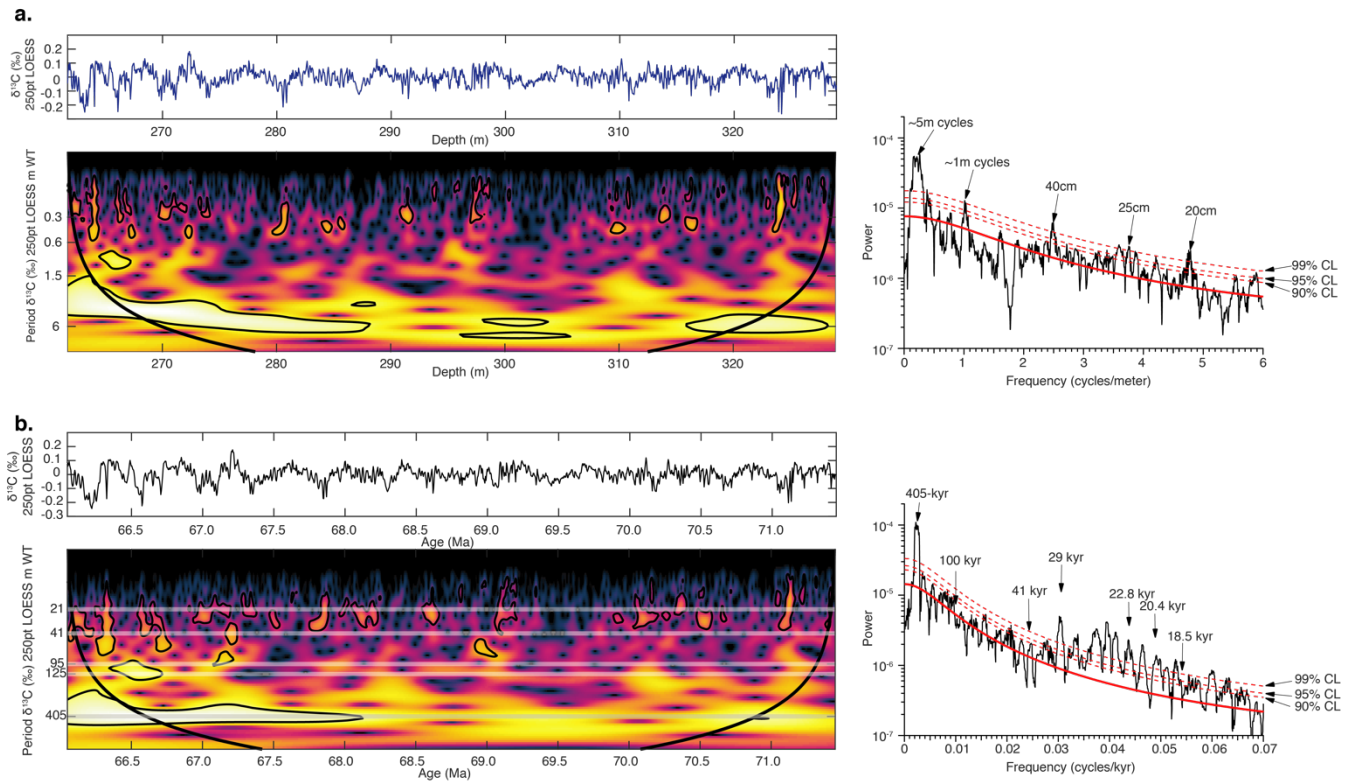
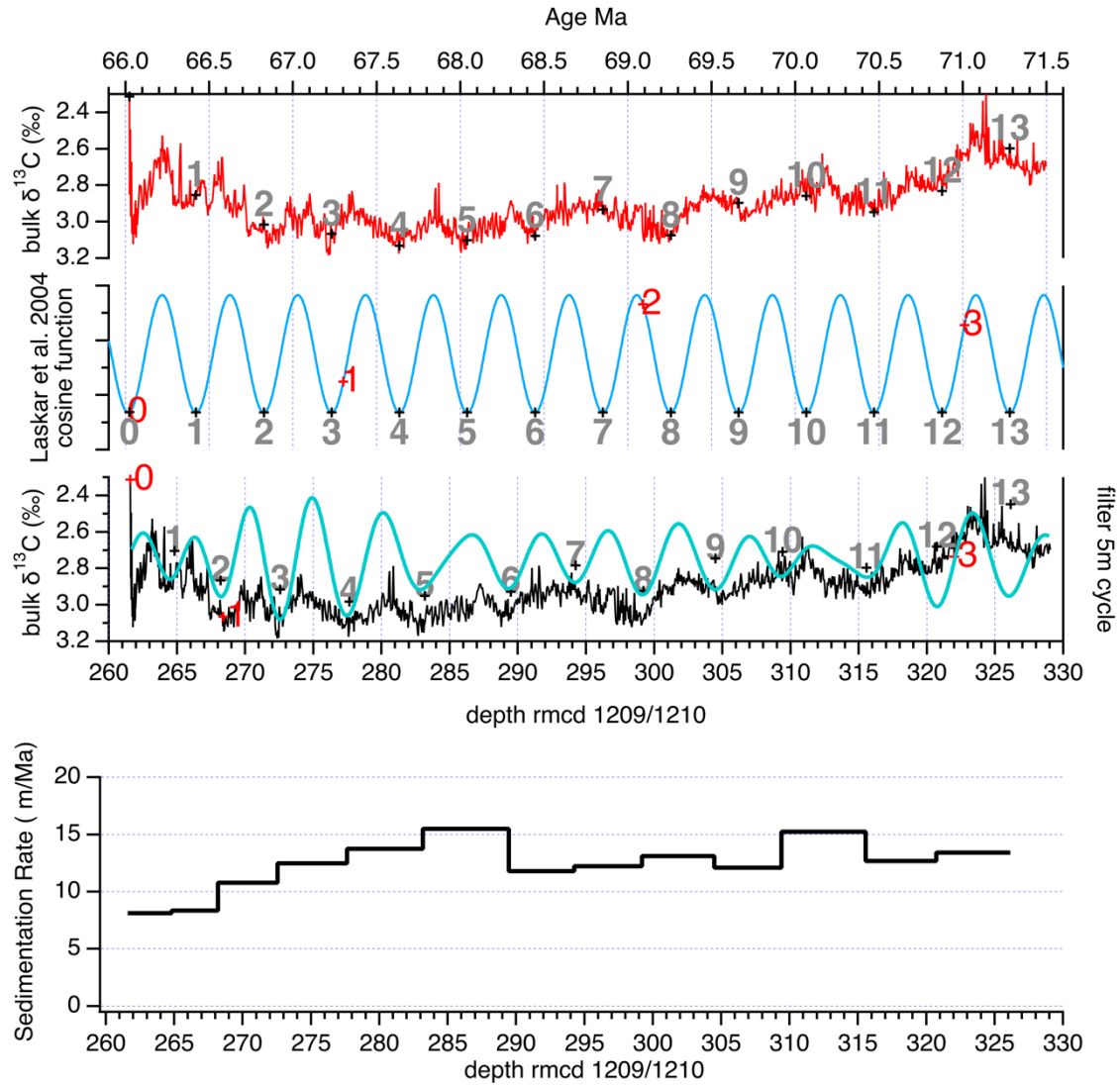


**Figure 2:** (a) Bulk carbonate  $\delta^{13}\text{C}$  by depth (m) shown with 250-point LOESS smoothing and wavelet analysis (Torrence and Compo, 1998; Grinsted et al., 2004), and multi-taper method (MTM) shown for spectral analysis. (b)  $\delta^{13}\text{C}$  by age (Ma) shown with 250-point LOESS smoothing and wavelet analysis, and MTM shown for spectral analysis. CL indicates confidence level. Note age is increasing from the left to right.

480





485 **Figure 3: (top)** Basic 405 kyr age model was first made by assigning Shatsky Rise Sites 1209 and 1210 composite bulk  $\delta^{13}\text{C}$  to known tie points (red numbers). Then, 5 m filter (bandpass  $0.2 \pm 0.06$ ) of bulk  $\delta^{13}\text{C}$  composite was modelled to know the cosine function (cyan line). This cosine function was correlated to La2004 Cosine function (Laskar et al., 2004; blue line) minima for tuning the depth to the stable 405 kyr cycle for an age. New Age is tie points in Supplement Table S4. **(bottom)** Sedimentation rate in meters per million years (m/Ma) of composite depth (rmcd).

490

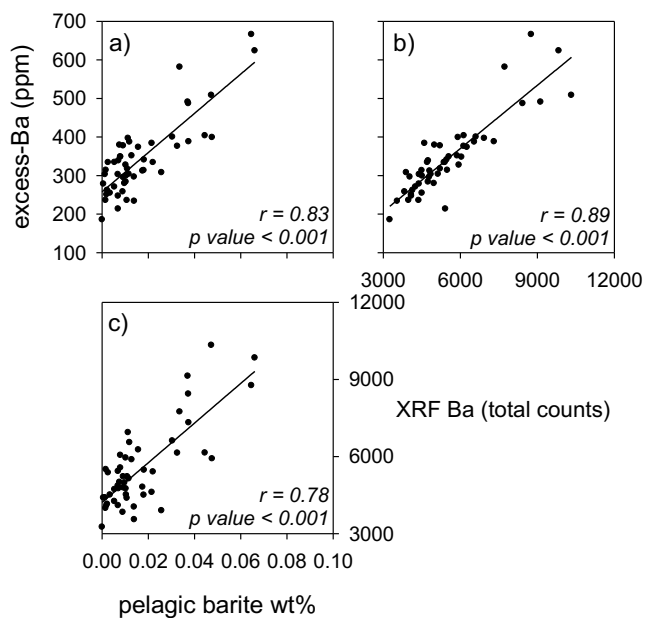


**Figure 4: Pelagic marine barite weight percent (wt %), excess-Ba (ppm), and XRF Ba (total counts) compared to each other. All correlations between barite related proxies are significant ( $p < 0.001$ ).**

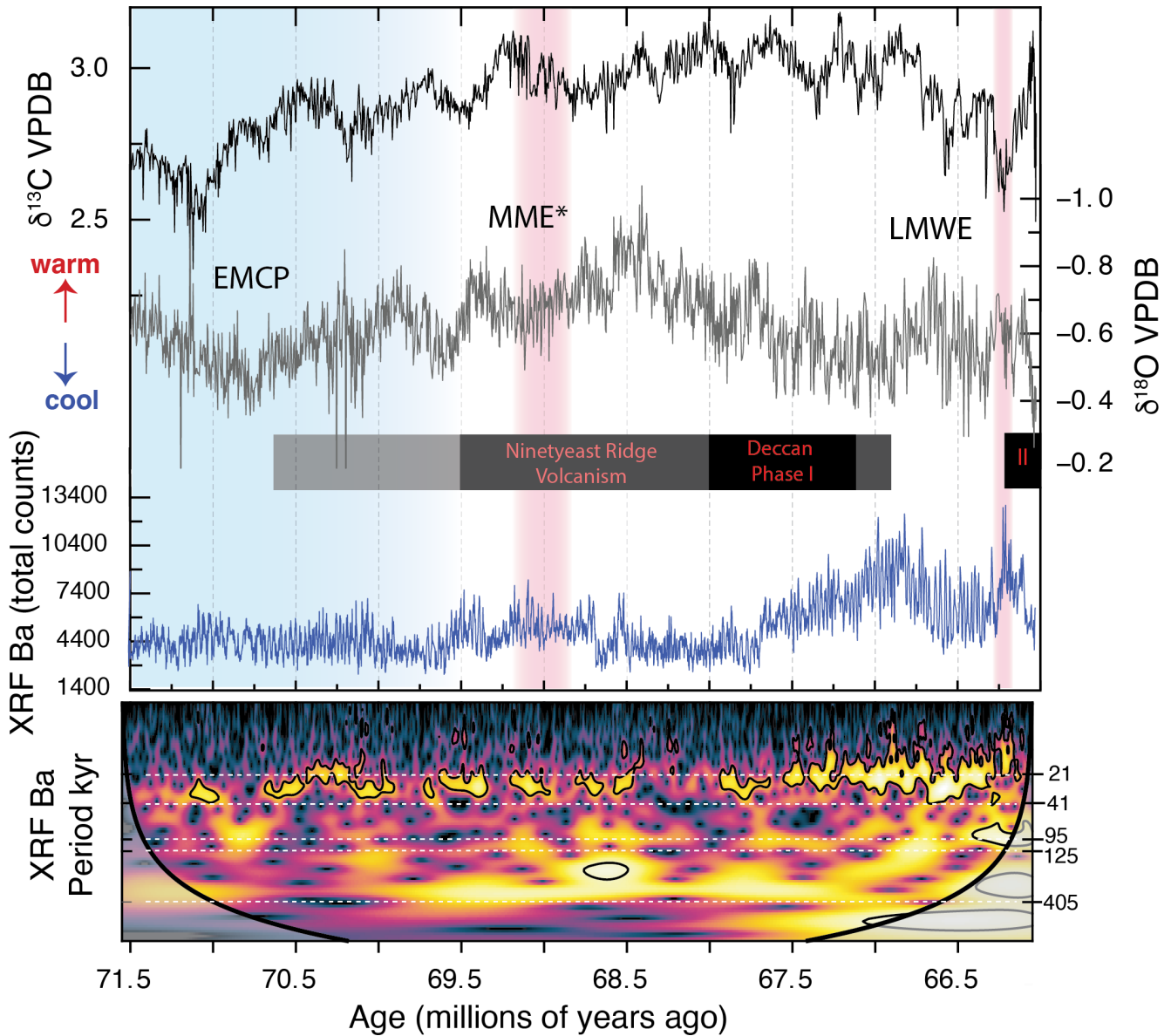
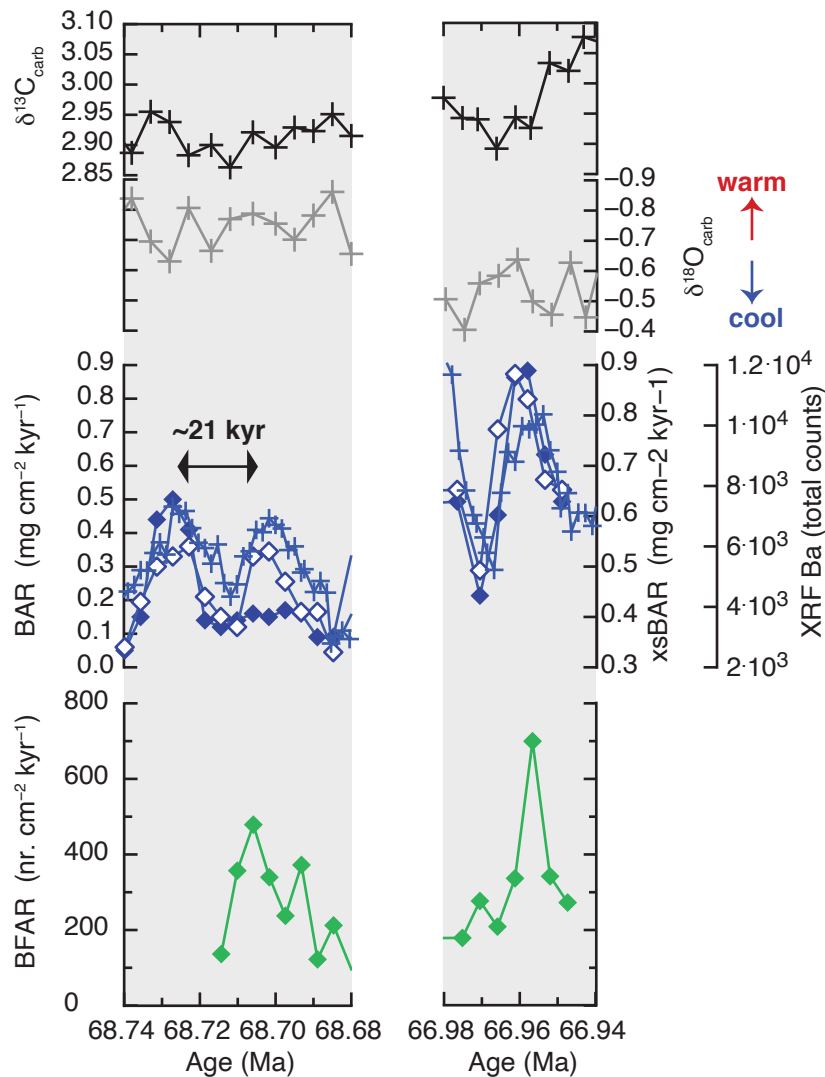


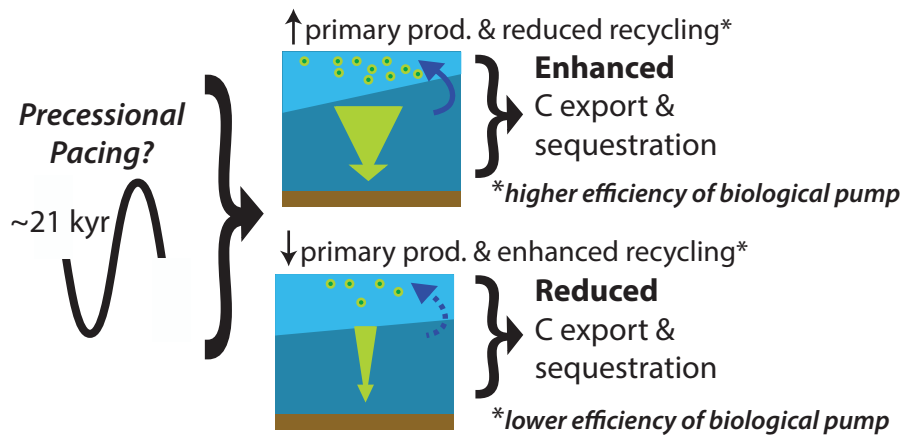
Figure 5: Bulk carbonate  $\delta^{13}\text{C}$ ,  $\delta^{18}\text{O}$ , scanning XRF Ba, and wavelet analysis (Torrence and Compo, 1998; Grinsted et al., 2004) on non-stationary periodicities for XRF Ba (500 loess composite of Sites 1209 and 1210) show signals of precession in scanning XRF Ba which strengthen after Deccan volcanism begins. Brighter colours correspond to higher power within a corresponding frequency period (in thousands of years or kyr). Ninetyeast hotspot volcanism and approximate duration of Deccan volcanism shown, adapted from Keller et al. (2016). EMCP = early Maastrichtian cooling pulse (Haynes et al., 2020); MME\* = mid-Maastrichtian event beginning at Chron C31n and lasting ~500kyr (Voigt et al., 2012); LMWE = latest Maastrichtian warming event (Li and Keller, 1998).

500

505



515 **Figure 6: Two discrete sample intervals covering potential cycles of precession (~21 kyr) with surface water related proxies (bulk  $\delta^{13}\text{C}$ ,  $\delta^{18}\text{O}$ ), organic carbon export proxies (scanning XRF Ba = crosses, excess-BaAR = open diamonds, and BAR = solid diamonds), and proxy for organic carbon arrival at the seafloor (BFAR = green diamonds). A positive correspondence is seen between carbon export from the surface of the oceans (XRF Ba, excess-BaAR, BAR) and organic carbon arrival at the seafloor (BFAR).**



525

Figure 7: Cycles of enhanced and reduced carbon (C) export and sequestration result from precessional paced variations in primary productivity and recycling in surface waters (i.e., changes in the efficiency of the biological pump). A shallower thermocline (steeper boundary between light and dark blue waters) would result in increased primary production and reduced recycling in the surface waters due to changes in water column stratification, continental nutrient fluxes and upwelling intensity which increases nutrients (solid blue arrow) and enhances C export out of the surface waters (wide green arrow). A deeper thermocline (near horizontal boundary between light and dark blue waters) would result in reduced primary production and enhanced recycling in the surface waters due to reduced nutrient availability (dashed blue arrow) and reduces C export out of the surface waters (thin green arrow). This ENSO-like variability could have controlled carbon export in the Maastrichtian.

530